Role of interfacial contribution in the bulklike enhanced Dzyaloshinskii-Moriya interaction of [Co/Tb]$_N$ multilayers

Zhiyuan Zhao [1,2] Zhicheng Xie,[1,2] Yiming Sun [3] Yumin Yang,[1,2] Ying Cao,[1,2] Lei Liu [1,2] Dong Pan [1,2] Na Lei [3,*] Zhongming Wei,[1,2] Jianhua Zhao,[1,2] and Dahai Wei [1,2,†]

[1]*State Key Laboratory for Superlattices and Microstructures, Institute of Semiconductors, Chinese Academy of Sciences, Beijing 100083, China*
[2]*College of Materials Science and Opto-Electronic Technology, University of Chinese Academy of Sciences, Beijing 100049, China*
[3]*Fert Beijing Institute, MIIT Key Laboratory of Spintronics, School of Integrated Circuit Science and Engineering, Beihang University, Beijing 100191, China*

Recently, magnetic multilayers composed of repetitive heavy metal/ferromagnetic bilayers have been extensively studied due to their large Dyzaloshinskii-Moriya interaction (DMI) and perpendicular magnetic anisotropy, which are considered key parameters to stabilize skyrmions at room temperature. However, the limitations of characterizing the ultrathin interfacial properties hinder the understanding of the microscopic origin of DMI. Here we report a bulklike enhancement of DMI strength (D) through the number of stacking layers (N) in [Co/Tb]$_N$ multilayers without introducing heavy metals and observe the value $1.38\,\mathrm{mJ/m^2}$ of D at $N = 8$. Using a phenomenological model, we attribute this bulklike behavior of D mainly to the increase in net interfacial DMI (iDMI) with N. The increase of iDMI is strongly correlated with the growth of the gradient in crystallographic asymmetry for adjacent interfaces during the stacking process. This structural phase transition concerning iDMI is demonstrated by the energy dispersive x-ray spectroscopy measurements and the N dependence of the longitudinal resistivity. We suggest that the asymmetrical distribution of Tb atoms breaks interfacial symmetry, leading to enhanced deviations in the crystallographic qualities for the top Tb/Co and bottom Co/Tb interfaces, resulting in an increase of the iDMI as N grows. Our findings suggest the potential of rare-earth transition-metal based magnetic multilayers for skyrmion applications due to their tunable magnetic properties regarding magnetic chiral textures.

I. INTRODUCTION

Broken inversion symmetry and spin-orbit coupling (SOC) in heterostructures of heavy metals (HMs) and ferromagnets (FMs) result in the Dzyaloshinskii-Moriya interaction (DMI) [1,2]. DMI competes with magnetic anisotropy, Heisenberg exchange interaction, and dipolar interaction thereby facilitating the formation of chiral Néel domain walls [3,4] and skyrmions [5,6]. Due to the potential for acquiring sizable DMI as well as applicability in skyrmions, recent studies concerning DMI have intensively focused on magnetic multilayers with repetitive HM/FM bilayers [7–10]. In these magnetic multilayers, SOC is generated by heavy metal and investigations of DMI are mainly focused on the broken inversion symmetry, namely, correlation between DMI and asymmetric crystallographic interfaces. Through thermal annealing to fabricate asymmetric interfaces, net interfacial DMI is induced in [Py/Pt]$_{10}$ symmetrical multilayers [11]; Davydenko *et al.* observed that DMI in [Co/Pd(111)]$_N$ is caused by the unequal strain of bottom Pd/Co and top Co/Pd interfaces [12]. These findings centered the physical mechanism of DMI in magnetic multilayers on asymmetrical interfacial properties, such as the degree of intermixing and the density of stacking faults. Recent studies have revealed that DMI in sputtered superlattices, such as Pt/[Co/Pd]$_N$ [13] and [Pt/Co/Pd]$_N$ [14], where each layer is amorphous and consists of a few atomic layers, can also be modulated by the repeating number of stacking layers. So far, although Ham *et al.* have attributed this N dependence of DMI in [Pt/Co/Pd]$_N$ to the formation of the bulk-asymmetry band during the stacking process [14], because each layer is ultrathin, characterizing interfacial asymmetry properties in these materials is limited, and the specific role of asymmetry interfaces compared with volume to generate DMI is unclear.

On the other hand, rare earth (RE) elements are expected to exhibit large spin-orbit coupling (SOC) due to their partially filled f orbitals and are known to generate large DMI [15,16]. In fact, bulk DMI has been observed in the GdFeCo monolayer without heavy metals due to the large SOC of Gd and bulk-broken inversion symmetry in the film [17]. Furthermore, rare earth–transition metal (RE-TM) material systems exhibit a strong negative exchange interaction and tunable net magnetization. The competition between magnetic moments of the RE and TM sublattices enables the net magnetization of RE-TM alloys to be tuned via temperature or composition. Similarly, the parameters that affect magnetic chiral textures, such as demagnetization, magnetic anisotropy, and Heisenberg exchange interaction, can be adjusted.
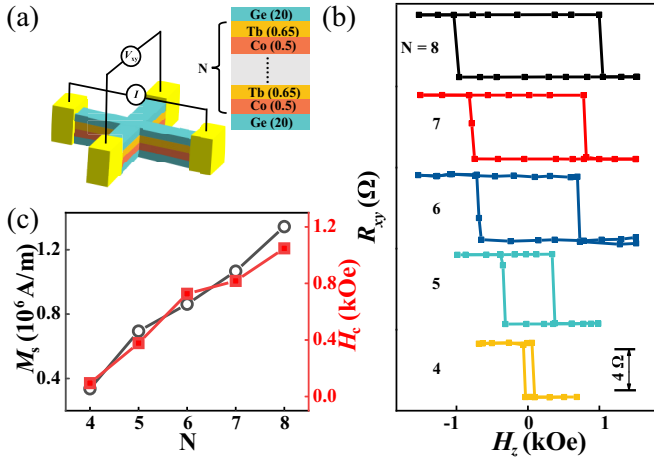
*na.lei@buaa.edu.cn
†dhwei@semi.ac.cn

FIG. 1. (a) Schematic illustrations of [Co/Tb]$_N$ multilayers and transport measurement setup on a Hall-bar device. (b) The transverse resistances (R_{xy}) of [Co(0.65)/Tb(0.5)]$_N$ with stacking number N from 4 to 8. (c) The net magnetizations (M_s) and coercivity fields (H_c) for the samples are plotted with stacking number N from 4 to 8.

Consequently, magnetic multilayers based on RE-TM material systems are expected to produce sizable DMI and tunable skyrmions for future investigations.

In this paper, we observe that the DMI of [Co/Tb]$_N$ multilayers without HM layers is enhanced by N and attains a value of $1.38 \, \text{mJ/m}^2$ when N is equal to 8. By using a phenomenological model, we clarify the volume and interface contributions of DMI. The net interfacial DMI (iDMI) on the adjacent Tb/Co and Co/Tb is separated and observed to increase with N. We have confirmed that as N increases, the increase of crystallographic asymmetry gradient for adjacent interfaces leads to an amplified net iDMI on each adjacent interface, supported by the observation of an asymmetric atom distribution via energy-dispersive x-ray spectroscopy.

II. SAMPLE PREPARATION AND CHARACTERIZATION

For this study, the magnetic multilayers of Ge(10)/ [Co(0.65)/Tb(0.5)]$_N$/Ge(10) are prepared by magnetron sputtering on thermally oxidized Si substrates with a base pressure of 5×10^{-8} Torr, as shown in Fig. 1(a); all thicknesses are in nm and N is the stacking number of [Co/Tb] unit. The thickness of each layer is determined by the precalibrated deposition rates and deposition time. The Ge layers with weak SOC are employed as buffers and protecting cap layers at the bottom and top, respectively. The films are further patterned into Hall bar devices with a size of 20 μm × 60 μm by using photolithography and ion milling. The schematic illustrations of the device and transport measurement setup are shown in Fig. 1(a).

Measurements of the anomalous Hall effect (AHE) are shown in Fig. 1(b). All samples reveal rectangular hysteresis loops with negative anomalous Hall resistance. In the RE-TM ferrimagnet, the anomalous Hall effect mainly derives from the spin-dependent scattering of $3d$ electrons in TM atoms, i.e., the Co, since the $4f$ band of the RE element is far below the Fermi level. In [Co(0.65)/Tb(0.5)]$_N$, the total

net magnetization (M_s) is dominated by the Tb and opposite to that of Co, resulting in the negative sign of anomalous Hall resistance. A similar negative anomalous Hall effect has been reported in the Tb-rich CoTb amorphous single layer [18]. The perpendicular magnetic anisotropy (PMA) can be clearly seen from $N = 4 - 8$. Black circles in Fig. 1(c) are the N dependence of net magnetization per unit magnetic layer volume (M_s), measured by a superconducting quantum interference device; the red squares in Fig. 1(c) are coercivity fields (H_c) extracted from anomalous Hall measurements and plotted with N. As depicted in Fig. 1(c), M_s exhibits a linear increase proportional to N. It has been reported that the distribution of RE and TM atoms in RE-TM materials can be altered by layer thickness, which impacts the effective composition of RE and TM elements. Therefore, the submoments could be alternated by layer thickness [19]. Given that the net magnetization within the samples is predominantly influenced by Tb submoments from analysis of Fig. 1(b), an increase in the relative concentration of Tb will result in a corresponding boost in the net magnetization. Moreover, H_c is observed to increase with N in Fig. 1(c), which is similar to the results observed in [Co/Gd]$_N$. The increase of interfacial alloying induced by N leads to a simultaneous rise in pinning centers for the domain wall, thus the increase of the coercivity fields with N is observed [20]. For this work, the increase of H_c with N could indicate a corresponding increase in the scale of interfacial alloying.

III. RESULTS AND DISCUSSION

To obtain relevant parameters for calculating the DMI strength in samples with different values of N, we first extract the DMI effective field (H_{DMI}) from the method based on the variation of domain wall energy in magnetic droplets [21]. As shown in the inset of Fig. 2(b), the hysteresis loops are performed by sweeping the external magnetic field (H_{ex}) with the tilted angle θ to obtain the magnetization switching field (H_{sw}). For a pinned domain wall with magnetization M_s toward H_{ex}, the depinning process and the shift of the domain wall (dx) occur when the change of Zeeman energy, $dE_Z = 2\mu_0 M_s H_{\text{ex}} \cos\theta \, dx$, is greater than the change of domain wall energy, dE_{DW}. Note that the domain wall energy can be affected by the deformation of the domain wall at the pinning center. The equating of these two energies yields the magnetization switching field required to move the pinned domain wall, given by $H_{\text{sw}} = (\frac{1}{2\mu_0 M_s} \frac{dE_{\text{DW}}}{dx}) \frac{1}{\cos\theta}$. Here, $\frac{1}{2\mu_0 M_s} \frac{dE_{\text{DW}}}{dx}$ is known as the coercivity field at $\theta = 0$ (H_c^0) [22]. The representative anomalous Hall resistance of the samples with $N = 5$ at different angles θ is shown in Fig. 2(a). H_{sw} is obtained from each θ and plotted in Fig. 2(b). For small angles ($0° < \theta < 60°$), H_{sw} closely follows $H_{\text{sw}} = H_c^0 / \cos\theta$, as depicted by the red solid line in Fig. 2(b) suggesting the depinning process of the domain wall. As θ increases, H_{sw} deviates the fitting, as shown in the red dashed line of Fig. 2(b) implying the type of domain wall at the pinning center is changed. Further, as Kim *et al.* have concluded, smaller in-plane fields applied on a magnetic droplet (given by $H_x = H_{\text{sw}} \sin\theta$ in this work) cannot overcome H_{DMI}, therefore the linear Néel domain wall is maintained. The domain wall energy also remains constant for this case. When H_x is larger than H_{DMI}, the linear Néel domain wall changes and the decrease of domain wall
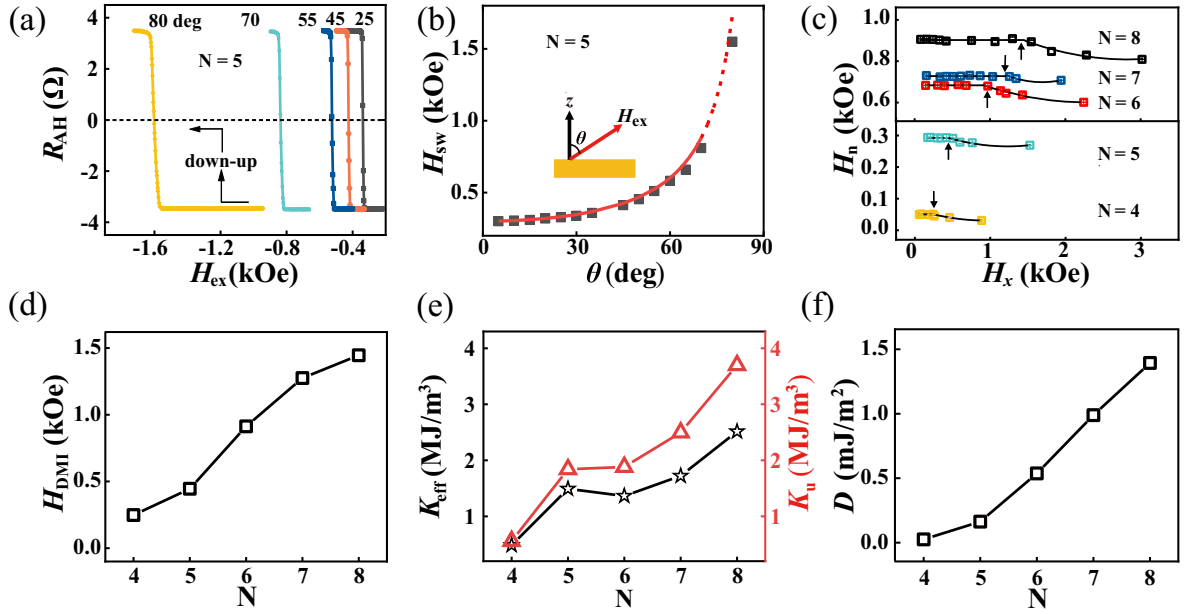
FIG. 2. (a) The representative anomalous Hall resistance of the sample with $N = 5$ with the external magnetic field (H_{ex}) applied at different tilted angles θ as illustrated in the inset of (b). (b) The magnetization switching field (H_{sw}) is plotted with θ for $N = 5$. The red line is the fitting line of $H_{sw} = H_c^0 / \cos\theta$, according to the Kondorsky model. (c) The nucleation field (H_n) is plotted with the in-plane field (H_x) for the samples with N. H_{DMI} is extracted from the threshold of H_x denoted by the black arrows. (d) The DMI effective fields (H_{DMI}) increase with the stacking number N. (e) The effective magnetic anisotropy energy (K_{eff}) and uniaxial magnetic anisotropy energy (K_u) are plotted with N. As N increases, both K_{eff} and K_u are enhanced. (f) The DMI strength (D) plotted with the stacking number N and observed to increase with N.

energy is expected [21]. Thus, H_{DMI} can be extracted from the correlation between domain wall energy and H_x. Note that this method for measuring H_{DMI} is similar to the method based on asymmetric domain dynamics. Both methods involve applying an in-plane magnetic field to break the chirality of the domain wall, which is maintained by DMI [23].

The square of domain wall energy is linearly proportional to the nucleation field, defined as $H_n = H_{sw}\cos\theta$ for this measurement [24]. To evaluate the threshold value of H_x, defined as $H_{sw}\sin\theta$, H_n is plotted as a function of H_x for the samples with different N, as shown in Fig. 2(c). When H_x increases, H_n maintains a constant value at first. As H_x increases to a threshold, H_n decreases monotonically with H_x, indicating H_{DMI} is canceled and the linear Néel domain wall is changed [21]. These results enable us to extract H_{DMI} from the threshold value of H_x marked by the arrows in Fig. 2(c). As depicted in Fig. 2(d), DMI effective field (H_{DMI}) monotonically increases with the stacking number N from 4 to 8.

Another critical parameter to calculate DMI strength is the effective perpendicular magnetic anisotropy (K_{eff}), given by $K_{eff} = H_K M_s/2$, where H_K is the magnetic anisotropy field, extracted from the in-plane R_{xy} measurements using the Stoner-Wohlfarth theory, given by $R_{xy} \propto M\sqrt{1 - (H/H_K)^2}$ [25]. As shown in Fig. 2(e), K_{eff} is observed to be $0.48\,\mathrm{MJ/m^3}$ for $N = 4$, reflecting a weak PMA. As the stacking number increases, K_{eff} rapidly increases, indicating that the PMA of the samples is enhanced; reaching $2.51\,\mathrm{MJ/m^3}$ for $N = 8$. K_{eff} can be further expressed as $K_{eff} = K_u - 2\pi M_s^2$, containing the uniaxial magnetic anisotropy (K_u) which originates from the interfacial anisotropy in HM/FM bilayers with broken symmetry, and the demagnetization effect, represented by $-2\pi M_s^2$ [25]. By subtracting the demagnetization effect, K_u for

different N are plotted in Fig. 2(e) and share the same tendency as K_{eff}. Generally, it has been established that in HM/FM heterostructures, the hybridization of interfacial electron orbitals results in a deviation between the out-of-plane and in-plane orbital magnetic moments, leading to interfacial magnetic anisotropy (K_s). This is described as follows: $K_s \propto (m_o^\perp - m_o^\parallel)$, where $m_o^\perp(m_o^\parallel)$ is the perpendicular (in-plane) orbital magnetic moments located in the first FM atom layer adjacent to the interface, known as Bruno's model [26–28]. For the $[Co/Tb]_N$, the addition of interfacial magnetic anisotropy is reasonable to contribute to the uniaxial magnetic anisotropy energy. On the other hand, RE-TM materials are reported to have volume magnetic anisotropy (K_v), which is correlated to RE-TM neighbor pairs in the vertical direction. Specifically, Harris et al. found that PMA in Fe-Tb is strongly correlated with out-of-plane Fe-Tb near neighbor pairs [29]. Further, Hufnagel observed a weakening of PMA after annealing FeTb alloys, which is attributed to redistribution of Fe-Tb pairs [30]. For the sample with the ideal symmetrical interface, K_v can be neglected; however, if an asymmetric atom distribution of Co and Tb atoms is induced during the stacking process, the formation of Co-Tb near neighbor pairs is expected, and the contribution of K_v to K_u should be considered.

Then we focus on the effective DMI strength (D) for samples with different stacking numbers from 4 to 8. D is calculated by $D = \mu_0 \Delta H_{DMI} M_s$ where μ_0 is the vacuum permeability, $\Delta = \sqrt{A/K_{eff}}$ is the domain wall width, and A is the exchange stiffness constant taken as $A(T) \propto M_s^{1.8}$ [31] with 1×10^{-11} J/m for $N = 4$ [32]. Note that the demagnetization effect has been included in the D of the magnetic thin film via the term K_{eff}. As shown in Fig. 2(f), D is nearly zero for $N = 4$ and monotonically increases with N from 4 to 8, reaching a
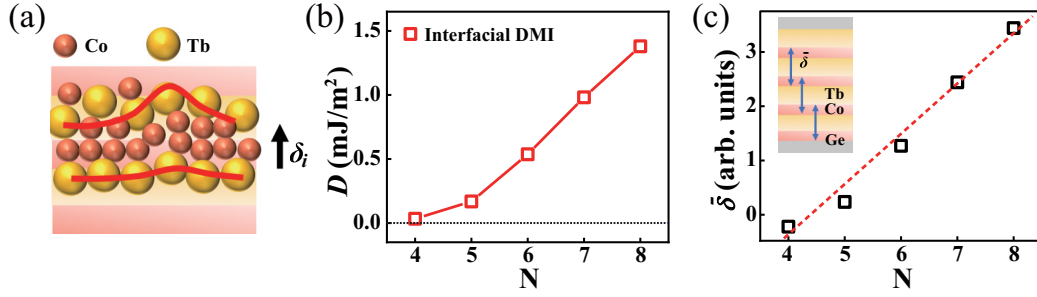
FIG. 3. (a) Illustration of gradient in the crystallographic asymmetry δ_i. (b) The interfacial contribution of DMI is plotted against N. (c) The average gradient interfacial crystallography quality $\bar{\delta}$, extracted from Eq. (2), plotted with N.

value of $1.38 \, \text{mJ/m}^2$ for $N = 8$. Notably, we have achieved this enhanced effective DMI strength in sputtered $[\text{Co/Tb}]_N$ without introducing heavy metals to generate a large spin-orbit coupling, making it compatible with the high-speed and large-scale integrated circuit manufacturing process [33–35].

As N grows, the total thickness of magnetic layers also increases. The enhancement of D with increasing total layer thickness reveals a bulklike behavior. A report of the bulk-like SOC related physical effect are observed in $L1_0-\text{FePt}$, where the spin-orbit torques are demonstrated to originate from the inherent structural gradient along the perpendicular direction of the film [36]. However, in the $[\text{Co/Tb}]_N$ multilayer, which consists of Co/Tb and Tb/Co interfaces, both interfacial and bulk contributions need to be considered to generate D. Namely, it is reasonable to assume that the interfacial disorders including atom intermixing are introduced during the layer-by-layer stacking process, which is expected to generate varied interfacial DMI (iDMI) on the Co/Tb and Tb/Co interfaces. The cancellation of unequal interfacial DMI on adjacent interfaces results in a net iDMI. On the other hand, a bulk-broken inversion symmetry induced by segregation of Tb and Co atoms is expected, which results in a volume DMI. Thus, further experimental evidence is necessary to uncover the physical mechanism for the bulk-like enhancement of DMI in $[\text{Co/Tb}]_N$.

IV. DISCUSSION

To separate interface and volume contributions from the increasing DMI strength, we propose a toy model for $[\text{Co/Tb}]_N$ where each Tb layer is embedded between two Co layers and the number of Co/Tb-Tb/Co adjacent interfaces is $N-1$. Considering the coexistence of both interfacial and volume contributions, the effective DMI strength per square meter (D) can be expressed as the following equation:

$$D(N) = \left[\sum_i^{N-1} \left(D_{\text{Co/Tb}}^{\text{bottom},i} - D_{\text{Tb/Co}}^{\text{top},i} \right) \right]/N + D_{\text{Co/Tb}}^{\text{top}}$$
$$+ D_v(t_{\text{Co}} + t_{\text{Tb}}), \tag{1}$$

where $D_{\text{Tb/Co}}^{\text{top},i}$ and $D_{\text{Co/Tb}}^{\text{bottom},i}$ are the interfacial DMI for each top Tb/Co and bottom Co/Tb adjacent interfaces, N is the number of Co/Tb repetitive unit, D_v is the volume DMI per cubic meter, and t_{Co} (t_{Tb}) is the thickness of the Co (Tb) layer, with 0.65 (0.5) nm. Since the interfacial DMI (iDMI)

is sensitive to the gradient of interfacial crystallographic quality [11,12], defined as δ_i and shown in Fig. 3(a), $D_{\text{Tb/Co}}^{\text{top},i}$ and $D_{\text{Co/Tb}}^{\text{bottom},i}$ can be written as $D_0(1 - \delta_i/2)$ and $D_0(1 + \delta_i/2)$ respectively, where D_0 is iDMI for symmetrical Co/Tb and Tb/Co interfaces, estimated as $0.44 \, \text{mJ/m}^2$ [37,38]. Assuming $D_{\text{Co/Tb}}^{\text{top}}$ equals D_0, Eq. (1) can be written as follows:

$$D(N) = \left(D_0 \sum_i^{N-1} \delta_i + D_0 \right)/N + D_v(t_{\text{Co}} + t_{\text{Tb}}). \tag{2}$$

Here, the interfacial crystallographic quality gradient δ_i could be extracted by subtracting the volume contributions of DMI from $D(N)$.

First, we focus on the volume contribution of DMI, D_v. The volume DMI generated by elemental segregation has been reported as a constant value with approximately $2.34 \times 10^{-3} \, \text{MJ/m}^3$ in bulk GdFeCo [17]. For the GdFeCo alloys with the maximum thickness less than 10 nm, the volume DMI induced by elemental segregation is neglectable and estimated to be smaller than $0.022 \, \text{mJ/m}^2$. In 6-nm FeGd and CoPt thin films with the composition gradient of 52%, DMI is not reported in FeGd and is observed to be smaller than $0.16 \, \text{mJ/m}^2$ in CoPt alloy [39]. Therefore, even though the $[\text{Co/Tb}]_N$ multilayer with the maximum thickness of 9.2 nm is entirely alloyed to form a CoTb monolayer with a composition gradient, similar to the situation for bulk GdFeCo and FeGd, the volume contribution of DMI could still be neglected compared with the measured effective D.

Here, the material system used in $[\text{Co/Tb}]_N$ multilayer is similar to the bulk GdFeCo. In both systems, the RE elements of Tb and Gd are responsible for providing spin-orbit coupling (SOC), and submoments on the RE and TM atoms are anti-ferromagnetically coupled. As a result, we adopt the volume DMI for every cubic meter as $2.34 \times 10^{-3} \, \text{MJ/m}^3$. As shown in the open blue squares of Fig. 3(b), the volume contribution per square meter, $D_v(t_{\text{Co}} + t_{\text{Tb}})$, is smaller than D for each N. The interfacial contribution of DMI is given by subtracting $D_v(t_{\text{Co}} + t_{\text{Tb}})$ from D and is observed to decrease with N, as shown in the open red squares of Fig. 3(b). The interfacial DMI becomes zero at $N = 4$, indicating that the adjacent Co/Tb and Tb/Co interfaces are symmetrical and the gradient of interfacial crystallographic quality has vanished. Based on Eq. (2), the increase of interfacial DMI with N implies the enhancement of δ_i and the possibility of a structural phase transition. To evaluate the variation of δ_i with respect to N, we consider the average interfacial crystallographic quality
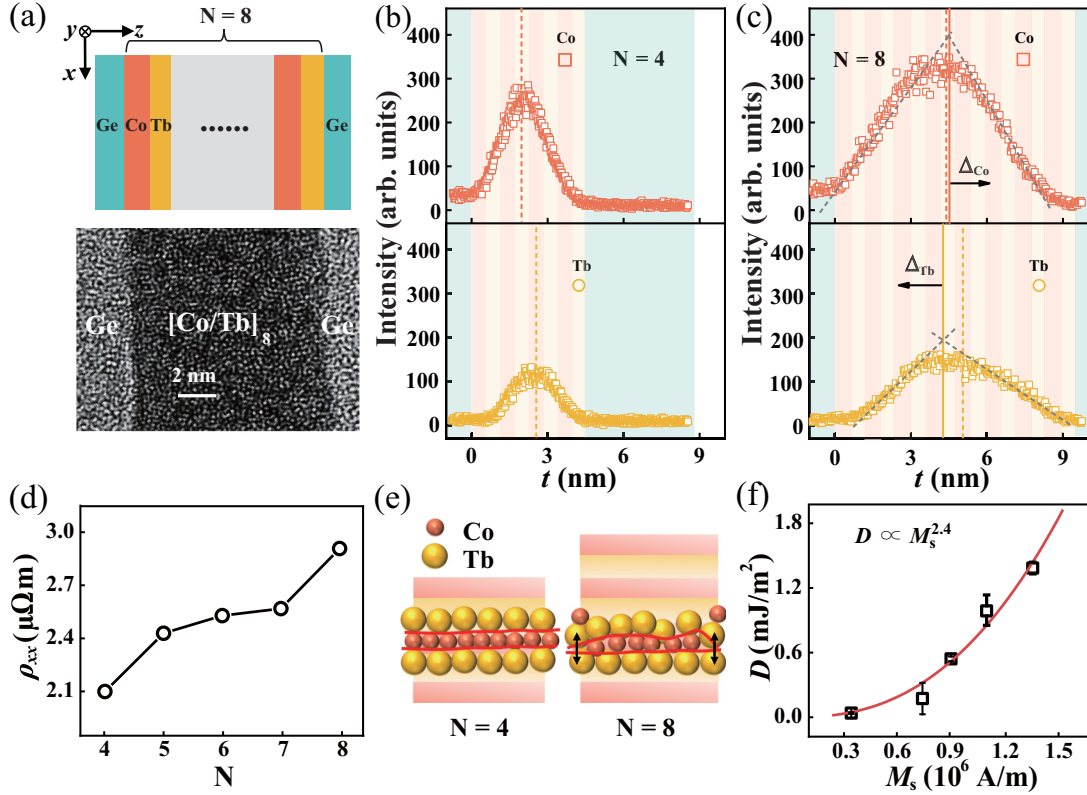
FIG. 4. (a) Top panel is the systematic illustration of the $x - z$ cross section in $[Co/Tb]_8$ superlattices. The bottom panel is high-resolution transmission electron microscopy (HRTEM) for the $[Co/Tb]_N$ with $N = 8$. The sample is amorphous. [(b),(c)] The top and bottom panels are the energy dispersive x-ray spectroscopy (EDS) plotted with the total layer thickness for Co (red open squares) and Tb (yellow open circles) with $N = 4$ and 8 respectively. Red and yellow dashed lines denote the geometric center for the Co and Tb stacks respectively. The deviation of Co and Tb peaks from the geometric centers are denoted in red and yellow solid lines respectively. (d) The dependence of the longitudinal resistivity (ρ_{xx}) on the stacking number N. (e) Illustration of formation process for gradient in the crystallographic asymmetry. (f) The dependence of D on the net magnetization M_s (open square dots) and correlated with $D \propto M_s^{2.4 \pm 0.1}$ (red solid line).

gradient $\bar{\delta}$, shown in the inset of Fig. 3(b), and given by $\bar{\delta} = \sum_i^{N-1} \delta_i / (N - 1)$ according to Eq. (2). As shown in Fig. 3(c), $\bar{\delta}$ grows with increasing N indicating that the deviation of the crystallographic quality between interfaces is enhanced. To demonstrate this structural phase transition inferred from the increase of interfacial DMI, we characterize the sample with $N = 4$ and 8 by the high-resolution transmission electron microscopy (HRTEM) and energy dispersive–x-ray spectroscopy (EDS).

In Figs. 4(a)–4(c), we characterize the HRTEM and EDS for the sample with $N = 4$ and 8 along the z direction, denoted by the axis in Fig. 4(a). As depicted in the bottom panel of Fig. 4(a), the long-range order is not expected in sputtered multilayer. The regions for Ge layers and $[Co/Tb]_N$ have been denoted inside. Figures 4(b) and 4(c) are EDS measurements plotted with the layer thickness (t) of $[Co/Tb]_N$ of Co (open squares) and Tb (open circles) atoms for $N = 4$ and 8 respectively. Despite the thicknesses of the Co and Tb monolayer layer being lower than the resolution of HRTEM and EDS that single layers cannot be distinguished, the average atom distributions of $[Co/Tb]_N$ could be reflected. Red and yellow dashed lines in Figs. 4(b) and 4(c) denote the geometric center for the Co and Tb stacks respectively. For $N = 4$, both the Co and Tb peaks are symmetrical, which indicates the symmetrical Co/Tb and Tb/Co interfaces. Deviation of

crystallographic qualities between interfaces could be neglected. However, for $N = 8$, the Co peak shifts towards the $+z$ direction, while the Tb peak obviously shifts towards the $-z$ direction. Assisted by the gray dashed lines, shifts of Co and Tb peaks are revealed and marked by the red and yellow dashed line in Fig. 4(c). The offsets of Co and Tb peaks from the geometric center, Δ_{Co} and Δ_{Tb}, are also denoted by the black arrows in Fig. 4(c). These results indicate the asymmetrical distributions of Co and Tb atoms along the $-z$ direction as N increases, which would break the well-defined Co/Tb and Tb/Co interfaces during the stacking process, and results in the increase of interfacial crystallographic quality gradient δ_i. Since iDMI is highly sensitive to the interfacial atomic structure [40], the enlarged deviation of interfacial crystallographic qualities would result in the increase of interfacial DMI.

Measurements of longitudinal resistivities (ρ_{xx}) for samples with different N could also demonstrate the increasing gradient in the crystallographic asymmetry of adjacent interfaces indirectly, as shown in Fig. 4(d). Typically, ρ_{xx} of the metallic thin film will decrease with the layer thickness, due to the decreasing scattering probability. In the case that the layer thickness exceeds the electron mean free path, ρ_{xx} is expected to remain constant [41]. However, for the $[Co/Tb]_N$, as the total layer thickness grows with N, an increase of ρ_{xx}

rather than the typical case is observed. This result indicates the growth of interfacial impurity scattering with N. We can infer that during the stacking process, due to atom intermixing and interfacial alloying, imperfect interfaces are formed.

Based on these results, we propose the microscopic origin for the bulklike enhancement of D in Fig. 4(e): for $N = 4$, the formation of well-defined interfaces is expected. Interfacial crystallographic qualities at Co/Tb and Tb/Co interfaces are uniform, which results in a vanished net iDMI for adjacent Co/Tb and Tb/Co interfaces. As N increases, due to the bonding energy of Tb-Tb being smaller than Co-Tb, Tb atoms from the upper layer tend to move toward the bottom and bind with Tb atoms inside. The asymmetrically distributed Tb and Co atoms would break the sharp interfaces and result in an increase of δ_i as well as the interfacial contribution of DMI. As N grows, despite a bulklike enhancement being observed, the effective D is still demonstrated to be dominated by the interfacial contribution induced by the gradient of interfacial crystallographic quality.

We also find that DMI increases with the magnetization (M_s) as depicted in Fig. 4(f) and fitted with $D \propto M_s^{2.4 \pm 0.1}$. One expects $D \propto M_s^2$, where M_s is the saturation magnetization, in a mean-field approximation, which is similar to the dependence $A \propto M_s^2$, where A is the exchange stiffness constant, by neglecting the Callen-like fluctuation corrections [42]. Further, the experimental efforts and the expression $A_{ij} \propto D_{ij} M_s/(2g)$, where g is the Landé g factor, derived by Liechtenstein *et al.* [43], have suggested that DMI shares the same physics with the Heisenberg exchange interaction. The smaller power component, 2.4 ± 0.1, compared with that of HM/FM heterostructures, for instance, 5.25 for the Pt/Co bilayer [37] and 4.9 for the $[Pt/Co/Cu]_{15}$ heterostructure [44], would be attributed to the smaller Heisenberg exchange integral of Co-Tb (RE-TM) moments compared with that of Co-Co (TM-TM) moments [45,46].

V. SUMMARY

In conclusion, we systematically investigated the Dzyaloshinskii-Moriya interaction as a function of stacking numbers $[Co/Tb]_N$ without introducing heavy metals. DMI strength is observed to increase with N. The value $1.38 \, \mathrm{mJ/m^2}$ is observed for $N = 8$. Considering the volume contribution remaining constant, we observe that the net interfacial DMI for each adjacent Tb/Co and Co/Tb interface is enhanced by N, which is observed to be strongly correlated with the gradient of the interfacial crystallographic asymmetry δ_i for each adjacent Co/Tb and Tb/Co interface. Together with asymmetry atom distribution of Co and Tb atoms observed by EDS, we propose the formation process for δ_i: as N increases, due to the accumulation of interfacial disorder including atom intermixing, the deviation of interfacial crystallographic qualities between Tb/Co and Co/Tb is enlarged and the net iDMI therefore increases. Note that the key parameters to generate skyrmions, DMI and PMA, are enhanced by N in this work; $[Co/Tb]_N$ is therefore considered as an ideal candidate to fabricate skyrmions at room temperature. Further, due to the parameters related to magnetic chiral textures, including demagnetization, magnetic anisotropy, and Heisenberg exchange interaction, also being tunable in RE-TM materials, our results emphasize the promising prospect for RE/TM multilayers in future applications regarding skyrmions.

[1] I. Dzyaloshinsky, A thermodynamic theory of "weak" ferromagnetism of antiferromagnetics, J. Phys. Chem. Solids **4**, 241 (1958).

[2] T. Moriya, Anisotropic superexchange interaction and weak ferromagnetism, Phys. Rev. **120**, 91 (1960).

[3] P. P. J. Haazen, E. Murè, J. H. Franken, R. Lavrijsen, H. J. M. Swagten, and B. Koopmans, Domain wall depinning governed by the spin Hall effect, Nat. Mater. **12**, 299 (2013).

[4] J. Torrejon, J. Kim, J. Sinha, S. Mitani, M. Hayashi, M. Yamanouchi, and H. Ohno, Interface control of the magnetic chirality in CoFeB/MgO heterostructures with heavy-metal underlayers, Nat. Commun. **5**, 4655 (2014).

[5] J. Sampaio, V. Cros, S. Rohart, A. Thiaville, and A. Fert, Nucleation, stability and current-induced motion of isolated magnetic skyrmions in nanostructures, Nat. Nanotechnol. **8**, 839 (2013).

[6] W. Jiang, P. Upadhyaya, W. Zhang, G. Yu, M. B. Jungfleisch, F. Y. Fradin, J. E. Pearson, Y. Tserkovnyak, K. L.Wang, O. Heinonen, S. G. E. Velthuis, S. G. E. te Velthuis, and A. Hoffmann, Blowing magnetic skyrmion bubbles, Science **349**, 283 (2015).

[7] A. Kundu and S. Zhang, Dzyaloshinskii-Moriya interaction mediated by spin-polarized band with Rashba spin-orbit coupling, Phys. Rev. B **92**, 094434 (2015).

[8] H. Yang, G. Chen, A. A. C. Cotta, A. T. N'Diaye, S. A. Nikolaev, E. A. Soares, W. A. A. M., K. Liu, A. K. Schmid, A. Fert, and M. Chshiev, Significant Dzyaloshinskii-Moriya interaction at graphene-ferromagnet interfaces due to the Rashba effect, Nat. Mater. **17**, 605 (2018).

[9] S. Woo, K. Litzius, B. Krüger, M.-Y. Im, L. Caretta, K. Richter, M. Mann, A. Krone, R. M. Reeve, M. Weigand, P. Agrawal, I. Lemesh, M.-A. Mawass, P. Fischer, M. Kläui, and G. S. D. Beach, Observation of room-temperature magnetic skyrmions and their current-driven dynamics in ultrathin metallic ferromagnets, Nat. Mater. **15**, 501 (2016).

[10] W. Jiang, G. Chen, K. Liu, J. Zang, S. G. E. te Velthuis, and A. Hoffmann, Skyrmions in magnetic multilayers, Phys. Rep. **704**, 1 (2017).

[11] K. Ahmadi, F. Mahfouzi, L. Jamilpanah, M. Mohseni, T. Böttcher, P. Pirro, N. Kioussis, J. Åkerman, S. A. S. Ebrahimi, and S. M. Mohseni, Inducing Dzyaloshinskii-Moriya

interaction in symmetrical multilayers using post annealing, Sci. Rep. **12**, 11877 (2022).

[12] A. V. Davydenko, A. G. Kozlov, A. G. Kolesnikov, M. E. Stebliy, G. S. Suslin, Yu. E. Vekovshinin, A. V. Sadovnikov, and S. A. Nikitov, Dzyaloshinskii-Moriya interaction in symmetric epitaxial $[Co/Pd(111)]_N$ superlattices with different numbers of Co/Pd bilayers, Phys. Rev. B **99**, 014433 (2019).

[13] S. D. Pollard, J. A. Garlow, J. Yu, Z. Wang, Y. Zhu, and H. Yang, Observation of stable Néel skyrmions in cobalt/palladium multilayers with Lorentz transmission electron microscopy, Nat. Commun. **8**, 14761 (2017).

[14] W. S. Ham, A.-M. Pradipto, K. Yakushiji, K. Kim, S. H. Rhim, K. Nakamura, Y. Shiota, S. Kim, and T. Ono, Dzyaloshinskii-Moriya interaction in noncentrosymmetric superlattices, npj Comput. Mater. **7**, 129 (2021).

[15] Q. Y. Wong, C. Murapaka, W. C. Law, W. L. Gan, G. J. Lim, and W. S. Lew, Enhanced Spin-Orbit Torques In Rare-Earth $Pt/[Co/Ni]_2/Co/Tb$ Systems, Phys. Rev. Appl. **11**, 024057 (2019).

[16] K. Ueda, C.-F. Pai, A. J. Tan, M. Mann, and G. S. D. Beach, Effect of rare earth metal on the spin-orbit torque in magnetic heterostructures, Appl. Phys. Lett. **108**, 232405 (2016).

[17] D.-H. Kim, M. Haruta, H.-W. Ko, G. Go, H.-J. Park, T. Nishimura, D.-Y. Kim, T. Okuno, Y. Hirata, Y. Futakawa, H. Yoshikawa, W. Ham, S. Kim, H. Kurata, A. Tsukamoto, Y. Shiota, T. Moriyama, S.-B. Choe, K.-J. Lee, and T. Ono, Bulk Dzyaloshinskii-Moriya interaction in amorphous ferrimagnetic alloys, Nat. Mater. **18**, 685 (2019).

[18] R. Q. Zhang, L. Y. Liao, X. Z. Chen, T. Xu, L. Cai, M. H. Guo, Hao Bai, L. Sun, F. H. Xue, J. Su, X. Wang, C. H. Wan, Hua Bai, Y. X. Song, R. Y. Chen, N. Chen, W. J. Jiang, X. F. Kou, J. W. Cai, H. Q. Wu, F. Pan, and C. Song, Current-induced magnetization switching in a CoTb amorphous single layer, Phys. Rev. B **101**, 214418 (2020).

[19] M. Ishibashi, K. Yakushiji, M. Kawaguchi, A. Tsukamoto, S. Nakatsuji, and M. Hayashi, Ferrimagnetic compensation and its thickness dependence in TbFeCo alloy thin films, Appl. Phys. Lett. **120**, 022405 (2022).

[20] S. Vorobiov, I. Lytvynenko, T. Hauet, M. Hehn, D. Derecha, and A. Chornous, The effect of annealing on magnetic properties of Co/Gd multilayers, Vacuum **120**, 9 (2015).

[21] S. Kim, P.-H. Jang, D.-H. Kim, M. Ishibashi, T. Taniguchi, T. Moriyama, K.-J. Kim, K.-J. Lee, and T. Ono, Magnetic droplet nucleation with a homochiral Néel domain wall, Phys. Rev. B **95**, 220402(R) (2017).

[22] F. Schumacher, On the modification of the Kondorsky function, J. Appl. Phys. **70**, 3184 (1991).

[23] J. Yu, X. Qiu, Y. Wu, J. Yoon, P. Deorani, J. Besbas, A. Manchon, and H. Yang, Spin orbit torques and Dzyaloshinskii-Moriya interaction in dual-interfaced Co-Ni multilayers, Sci. Rep. **6**, 32629 (2016).

[24] S. Pizzini, J. Vogel, S. Rohart, L. D. Buda-Prejbeanu, E. Jué, O. Boulle, I. M. Miron, C. K. Safeer, S. Auffret, G. Gaudin, and A. Thiaville, Chirality-Induced Asymmetric Magnetic Nucleation in $Pt/Co/AlO_x$ Ultrathin Microstructures, Phys. Rev. Lett. **113**, 047203 (2014).

[25] C. Tannous and J. Gieraltowski, The Stoner-Wohlfarth model of ferromagnetism, Eur. J. Phys. **29**, 475 (2008).

[26] D. Yi, H. Amari, P. P. Balakrishnan, C. Klewe, A. T. N'Diaye, P. Shafer, N. Browning, and Y. Suzuki, Enhanced Interface-Driven Perpendicular Magnetic Anisotropy by Symmetry Control in Oxide Superlattices, Phys. Rev. Appl. **15**, 024001 (2021).

[27] D. Weller, J. Stohr, R. Nakajima, A. Carl, M. G. Samant, C. Chappert, R. Megy, P. Beauvillain, P. Veillet, and G. A. Held, Microscopic Origin of Magnetic Anisotropy in Au/Co/Au Probed with X-Ray Magnetic Circular Dichroism, Phys. Rev. Lett. **75**, 3752 (1995).

[28] P. Bruno, Tight-binding approach to the orbital magnetic moment and magnetocrystalline anisotropy of transition-metal monolayers, Phys. Rev. B **39**, 865 (1989).

[29] V. G. Harris, K. D. Aylesworth, B. N. Das, W. T. Elam, and N. C. Koon, Structural Origins of Magnetic Anisotropy in Sputtered Amorphous Tb-Fe Film, Phys. Rev. Lett. **69**, 1939 (1992).

[30] T. C. Hufnagel, S. Brennan, P. Zschack, and B. M. Clemens, Structural anisotropy in amorphous Fe-Tb thin films, Phys. Rev. B **53**, 12024 (1996).

[31] K. R. Coffey, T. Thomson, and J.-U. Thiele, Angular dependence of the switching field of thin-film longitudinal and perpendicular magnetic recording media, J. Appl. Phys. **92**, 4553 (2002).

[32] R. Mishra, J. Yu, X. Qiu, M. Motapothula, T. Venkatesan, and H. Yang, Anomalous Current-Induced Spin Torques in Ferrimagnets Near Compensation, Phys. Rev. Lett. **118**, 167201 (2017).

[33] Q. Liu, L. Zhu, X. S. Zhang, D. A. Muller, and D. C. Ralph, Giant bulk spin-orbit torque and efficient electrical switching in single ferrimagnetic FeTb layers with strong perpendicular magnetic anisotropy, Appl. Phys. Rev. **9**, 021402 (2022).

[34] H. Zhang, X. Ma, C. Jiang, J. Yin, S. Lyu, S. Lu, X. Shang, B. Man, C. Zhang, D. Li, S. Li, W. Chen, H. Liu, G. Wang, K. Cao, Z. Wang, and W. Zhao, Integration of high-performance spin-orbit torque MRAM devices by 200-mm-wafer manufacturing platform, J. Semicond. **43**, 102501 (2022).

[35] L. Chen, J. Zhao, D. Weiss, C. H. Back, F. Matsukura, and H. Ohno, Magnetization dynamics and related phenomena in semiconductors with ferromagnetism, J. Semicond. **40**, 081502 (2019).

[36] M. Tang, K. Shen, S. Xu, H. Yang, S. Hu, W. Lü, C. Li, M. Li, Z. Yuan, S. J. Pennycook, K. Xia, Aurelien Manchon, Shiming Zhou, and Xuepeng Qiu, Bulk spin torque-driven perpendicular magnetization switching in $L1_0$ FePt single layer, Adv. Mater. **32**, 2002607 (2020).

[37] Y. Zhang, X. Kong, G. Xu, Y. Jin, C. Jiang, and G. Chai, Direct observation of the temperature dependence of the Dzyaloshinskii-Moriya interaction, J. Phys. D: Appl. Phys. **55**, 195304 (2022).

[38] T. Lin, X. Zhang, N. Vernier, X. Wang, E. Dong, C. Chen, J. Niu, Y. Sun, L. Yang, W. Zheng, S. Du, N. Lei, and W. Zhao, Chiral morphology in ferrimagnetic Pt/Co/Tb bubble domains, Phys. Rev. B **106**, 184407 (2022).

[39] Q. Zhang, J. Liang, K. B. Le Zhao, H. Bai, Q. Cui, H.-A. Zhou, H. Bai, H. Feng, W. Song, G. Chai, O. Gladii, H. Schultheiss, T. Zhu, J. Zhang, Y. Peng, H. Yang, and W. Jiang, Quantifying the Dzyaloshinskii-Moriya Interaction Induced by the Bulk Magnetic Asymmetry, Phys. Rev. Lett. **128**, 167202 (2022).

[40] A. Hrabec, N. A. Porter, A. Wells, M. J. Benitez, G. Burnell, S. McVitie, D. McGrouther, T. A. Moore, and C. H. Marrows, Measuring and tailoring the Dzyaloshinskii-Moriya interaction

in perpendicularly magnetized thin films, Phys. Rev. B **90**, 020402(R) (2014).

[41] W. Zhang, S. H. Brongersma, O. Richard, B. Brijs, R. Palmans, L. Froyen, and K. Maex, Influence of the electron mean free path on the resistivity of thin metal films, Microelectron. Eng. **76**, 146 (2004).

[42] L. Rózsa, U. Atxitia, and U. Nowak, Temperature scaling of the Dzyaloshinsky-Moriya interaction in the spin wave spectrum, Phys. Rev. B **96**, 094436 (2017).

[43] A. I. Liechtenstein, M. I. Katsnelson, and V. A. Gubanov, Local spin density functional approach to the theory of exchange interactions in ferromagnetic metals and alloys, J. Phys. F: Met. Phys. **14**, L125 (1984).

[44] S. Schlotter, P. Agrawal, and G. S. D. Beach, Temperature dependence of the Dzyaloshinskii-Moriya interaction in Pt/Co/Cu thin film heterostructures, Appl. Phys. Lett. **113**, 092402 (2018).

[45] M. Mansuripur and M. F. Ruane, Mean-field analysis of amorphous rare earth-transition metal alloys for thermomagnetic recording, IEEE Trans. Magn. **22**, 33 (1986).

[46] Z. Zhao, D. Su, T. Lin, Z. Xie, D. Zhao, J. Zhao, N. Lei, and D. Wei, Separation of Rare-Earth and Transition-Metal Contributions to the Interfacial Dzyaloshinskii-Moriya Interaction in Ferrimagnetic Co-Gd Alloys, Phys. Rev. Appl. **19**, 044037 (2023).